Crack surface roughness in three-dimensional random fuse networks

Phani Kumar V. V. Nukala
Computer Science and Mathematics Division, Oak Ridge National Laboratory, Oak Ridge, Tennessee 37831-6164, USA

Stefano Zapperi
CNR, INFM, Dipartimento di Fisica, Università "La Sapienza", P.le A. Moro 2, 00185 Roma, Italy

Srđan Šimunović
Computer Science and Mathematics Division, Oak Ridge National Laboratory, Oak Ridge, Tennessee 37831-6164, USA

(Received 27 October 2005; published 3 August 2006)

Using large system sizes with extensive statistical sampling, we analyze the scaling properties of crack roughness and damage profiles in the three-dimensional random fuse model. The analysis of damage profiles indicates that damage accumulates in a diffusive manner up to the peak load, and localization sets in abruptly at the peak load, starting from a uniform damage landscape. The global crack width scales as $W \sim L^{0.5}$ and is consistent with the scaling of localization length $\xi \sim L^{0.5}$ used in the data collapse of damage profiles in the postpeak regime. This consistency between the global crack roughness exponent and the postpeak damage profile localization length supports the idea that the postpeak damage profile is predominantly due to the localization produced by the catastrophic failure, which at the same time results in the formation of the final crack. Finally, the crack width distributions can be collapsed for different system sizes and follow a log-normal distribution.

DOI: 10.1103/PhysRevE.74.026105 PACS number(s): 46.50.+a, 64.60.Ak, 62.20.Mk

I. INTRODUCTION

Understanding the scaling properties of fracture in disordered media represents an intriguing theoretical problem with some technological implications [1]. Experiments have shown that in several materials under different loading conditions the fracture surface is self-affine [2,3], and the out of plane roughness exponent, ζ, displays a universal value of $\zeta \simeq 0.8$ irrespective of the material studied [4]. In particular, experiments have been done in metals [5], glass [6], rocks [7], and ceramics [8], covering both ductile and brittle materials. However, the current understanding that has emerged is that crack roughness displays a universal value of $\zeta \simeq 0.8$ only at larger scales and at higher crack speeds, whereas another roughness exponent in the range of 0.4–0.6 is observed at smaller length scales under quasistatic or slow crack propagation [4].

It was later shown that the roughness exponent conventionally measured describes only the local properties, while the fracture surface instead exhibits anomalous scaling [9]: the *global* exponent describing the scaling of the crack width with the sample size is larger than the local exponent measured on a single sample [10,11]. It is thus necessary to define two roughness exponents: a global one (ζ) and a local one (ζ_{loc}). Only the latter appears to be universal, with a value of $\zeta_{loc} \simeq 0.8$ [4] that is independent of the material tested.

The theoretical understanding of the origin and universality of crack surface roughness is often investigated by discrete lattice (fuse, central-force, and beam) models. In these models the elastic medium is described by a network of discrete elements such as springs and beams with random failure thresholds. In the simplest approximation of a scalar displacement, one recovers the random fuse model (RFM), where a lattice of fuses with random threshold are subject to an increasing external voltage [12–18]. Using two-dimensional RFM, the estimated crack surface roughness exponents are $\zeta = 0.7 \pm 0.07$ [19], $\zeta_{loc} = 2/3$ [20], and $\zeta = 0.74 \pm 0.02$ [21]. Recently, using large system sizes (up to $L = 1024$) with extensive sample averaging, we found that the crack roughness exhibits anomalous scaling [22] similar to the recent experimental observations [9,23]. In particular, the local and global roughness exponents estimated using two different lattice topologies are $\zeta_{loc} = 0.72 \pm 0.02$ and $\zeta = 0.84 \pm 0.03$. In comparison, the roughness exponents obtained from experiments on quasi- two-dimensional materials are $\zeta = 0.73 \pm 0.07$ for collapsible cylindrical straws [24], $\zeta_{loc} = 0.68 \pm 0.04$ in thin wood planks [25], and $\zeta_{loc} \approx 0.73$ for crack lines in wet paper [26]. The numerical results obtained using two-dimensional RFM are in reasonable agreement with the above quasi two-dimensional experimental results.

However, there exists a huge discrepancy between the numerically computed roughness exponents using the three-dimensional (3D) RFM [27–29] and the experimentally observed universal value of $\simeq 0.8$. The roughness exponent was estimated to be $\zeta = 0.62 \pm 0.05$ in Ref. [27], whereas a much smaller exponent of $\zeta = 0.41 \pm 0.02$ was estimated in Refs. [28,29]. The measured roughness exponents in Refs. [28,29] are similar to the ones describing a minimum energy surface (or a directed polymer in $d = 2$), which would imply that crack formation occurs by an optimization process, but the issue is still controversial [27,29]. For the purpose of this paper, it is also worth noting that a roughness exponent of $\zeta = 0.5$ [30] is obtained using three-dimensional Born models.

II. MODEL

In the random thresholds fuse model, the lattice is initially fully intact with bonds having the same conductance, but the

bond breaking thresholds, t, are randomly distributed based on a thresholds probability distribution, $p(t)$. The burning of a fuse occurs irreversibly, whenever the electrical current in the fuse exceeds the breaking threshold current value, t, of the fuse. Periodic boundary conditions are imposed in both of the horizontal directions (x and y directions) to simulate an infinite system, and a constant voltage difference, V, is applied between the top and the bottom of the lattice system bus bars.

Numerically, a unit voltage difference, $V=1$, is set between the bus bars (in the z direction) and the Kirchhoff equations are solved to determine the current flowing in each of the fuses. Subsequently, for each fuse j, the ratio between the current i_j and the breaking threshold t_j is evaluated, and the bond j_c having the largest value, $\max_j \frac{i_j}{t_j}$, is irreversibly removed (burnt). The current is redistributed instantaneously after a fuse is burnt, implying that the current relaxation in the lattice system is much faster than the breaking of a fuse. Each time a fuse is burnt, it is necessary to recalculate the current redistribution in the lattice to determine the subsequent breaking of a bond. The process of breaking of a bond, one at a time, is repeated until the lattice system falls apart. In this work, we assume that the bond breaking thresholds are distributed based on a uniform probability distribution, which is constant between 0 and 1.

The failure response of the random fuse network is, however, well known to be highly sensitive to the choice of the threshold distribution [31]. However, as mentioned in [27], although some failure properties and exponents depend on the choice of thresholds distribution, others, notably the roughness exponents, appear to be universal and not depend on the choice of thresholds distribution. Since the primary focus of this work is to estimate the crack surface roughness using the 3D random fuse models, the results presented in this work based on uniform thresholds distribution are representative of earlier works [27,29], but with large system sizes and extensive statistical sampling.

Numerical simulation of fracture using large fuse networks is often hampered due to the high computational cost associated with solving a new large set of linear equations every time a new lattice bond is broken. Although the sparse direct solvers presented in [32] are superior to iterative solvers in two-dimensional (2D) lattice systems, for 3D lattice systems, the memory demands brought about by the amount of fill-in during the sparse Cholesky factorization favor iterative solvers. Hence, iterative solvers are in common use for large scale 3D lattice simulations. The authors have developed an algorithm based on a block-circulant preconditioned conjugate gradient (CG) iterative scheme [33] for simulating 3D random fuse networks. The block-circulant preconditioner was shown to be superior compared with the *optimal* point-circulant preconditioner for simulating 3D random fuse networks [33]. Since the block-circulant and optimal point-circulant preconditioners achieve favorable clustering of eigenvalues (in general, the more clustered the eigenvalues are, the faster the convergence rate is), these algorithms significantly reduced the computational time required for solving large lattice systems in comparison with the Fourier accelerated iterative schemes used for modeling lattice breakdown [27,34,35]. Using this numerical algorithm, we investigated fracture of large 3D cubic ($L\times L\times L$) lattice systems (e.g., $L=64$), which is so far the largest lattice system considered. For many lattice system sizes, the number of sample configurations, N_{config}, used are extremely large to reduce the statistical error in the numerical results. In particular, we used $N_{config}=50\,000, 20\,000, 2512, 1200, 400$, and 11 for $L=10$, 16, 24, 32, 48, and 64, respectively (see Table I).

TABLE I. A summary of the main results of the 3D RFM simulations for uniform thresholds distribution, including the number of configurations used to average the results for each system size. n_p and n_f denote the mean fraction of broken bonds in a lattice system of size L at the peak load and at failure, respectively. Similarly, Δ_p and Δ_f denote the standard deviation of fraction of broken bonds at the peak load and at failure, respectively.

L	N_{config}	Cubic			
		n_p	Δ_p	n_f	Δ_f
10	50 000	563	57	726	59
16	20 000	2108	147	2572	152
24	2512	6692	354	7882	337
32	1200	15 329	705	17 691	649
48	400	49 495	1582	55 768	1523
64	11	114 243	5704	127 040	5378

III. DAMAGE PROFILES

In the case of strong disorder, damage is diffusive in the initial stages of loading up to almost the peak load. Around the peak load, the damage starts to localize and ultimately leads to failure (see Fig. 1). Since the final breakdown event is very different from the initial precursors up to the peak load, we analyze the accumulated damage in the pre- and postpeak regimes. Figure 2 presents the average damage profiles $p(z)$ for different system sizes. The damage profile $p(z)$ is defined as the number of broken bonds $n_b(z)$ in each of the segments along the z direction and is computed as $p(z)=n_b(z)/[(3L+2)(L+1)]$ for each of the sample configurations. The averaging of the damage profiles is obtained by first shifting the damage profiles by the center of mass of the damage and then averaging over different samples. The results presented in Fig. 2 indicate that although the average damage profiles at smaller lattice system sizes are not completely flat, they flatten considerably as the lattice system size is increased. We tend thus to attribute the apparent profile to size effects. Indeed, for large system sizes, the results clearly show that there is no localization at the peak load. Consequently, the localization of damage is mostly due to the damage accumulated between the peak load and failure, i.e., the final catastrophic breakdown event. The damage profiles at the peak load exhibit similar behavior even in the 2D RFM [36] and random spring model [37]. A quadratic form of damage profiles was proposed in Refs. [34,35]; however, such apparent nonlinearity of damage profiles in Refs. [34,35] may be attributed to results based on small system

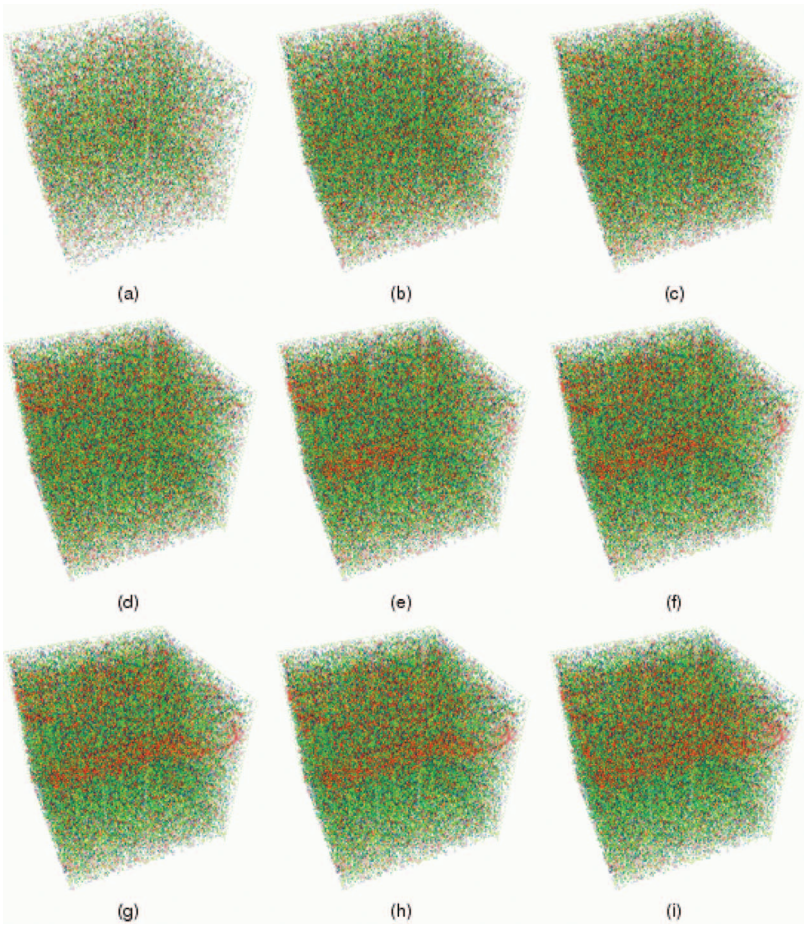

FIG. 1. (Color) Snapshots of damage in a typical cubic lattice system of size $L=64$. Number of broken bonds at the peak load and at failure are 114 845 and 126 577, respectively. (a)–(i) Snapshots of damage after breaking n_b number of bonds. The coloring scheme is such that in each snapshot, the bonds broken in the early stages are colored blue, then green, followed by yellow, and finally the last stage of broken bonds are colored red. (a) $n_b=50\,000$, (b) $n_b=100\,000$, (c) $n_b=114\,845$ (peak load), (d) $n_b=117\,000$, (e) $n_b=119\,000$, (f) $n_b=121\,000$, (g) $n_b=123\,000$, (h) $n_b=125\,000$, and (i) $n_b=126\,577$ (failure).

sizes (only systems up to $L=24$ were considered in [34,35]) and the method employed for averaging the damage profiles (see Ref. [36] for a detailed discussion).

Figure 3 presents the data collapse of the average damage profiles for the damage accumulated between the peak load and failure using a power law scaling. An excellent collapse

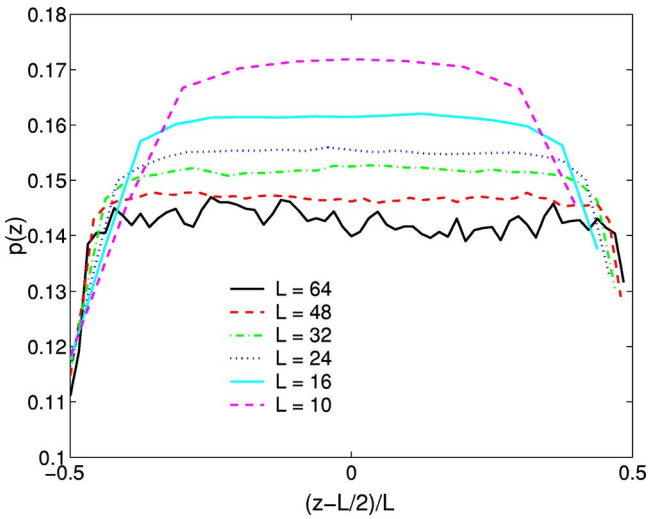

FIG. 2. (Color online) Average damage profiles at peak load obtained by first centering the data around the center of mass of the damage and then averaging over different samples.

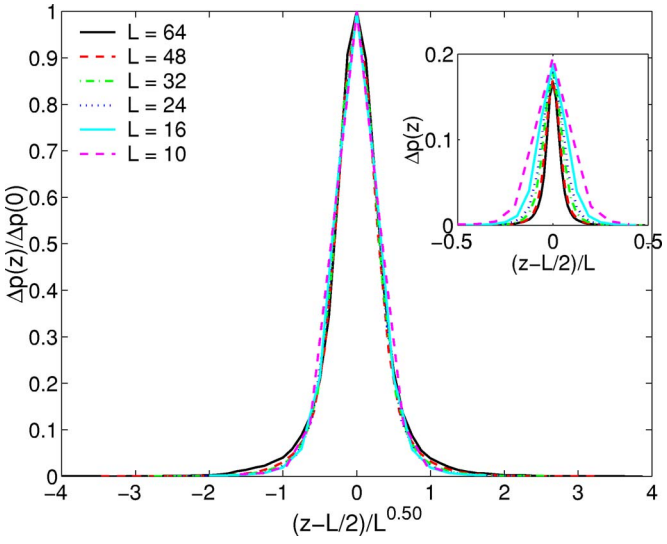

FIG. 3. (Color online) Data collapse of the average profiles for the damage accumulated between peak load and failure using a power law scaling. The profiles show exponential tails. Data collapse was not achieved using a linear scaling for the localization length. The inset shows the unscaled data of the average profiles, wherein the average has been performed after shifting by the center of mass.

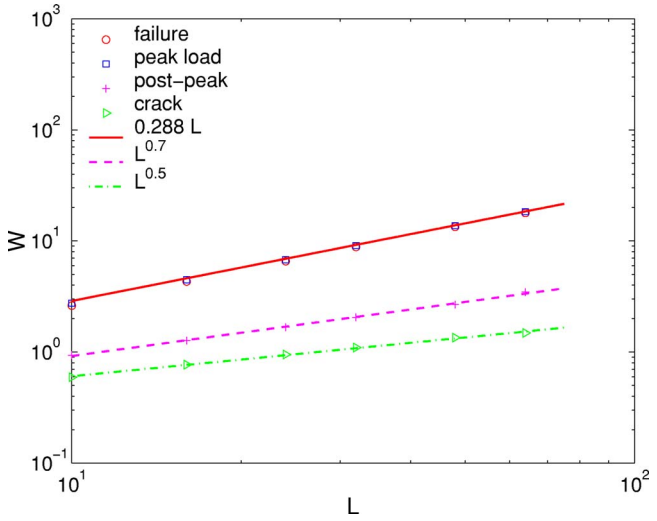

FIG. 4. (Color online) The damage width at peak load and at failure are basically the same. The linear scaling is expected for a uniform distribution and is not due to localization. On the other hand, localization can be observed for postpeak damage, and the width scales as a power law.

of the data is achieved using the scaling form

$$\langle \Delta p(z,L)\rangle / \langle \Delta p(0)\rangle = f(|z - L/2|/\xi), \tag{1}$$

where the damage peak scales as $\langle \Delta p(0)\rangle \sim L^{-0.15}$ and the localization length scales as $\xi \sim L^{\alpha}$, with $\alpha = 0.50$. The damage profiles decay exponentially at large system sizes. We have also tried a simple linear scaling of the form $\langle \Delta p(z,L)\rangle / \langle \Delta p(0)\rangle = f[(z - L/2)/L]$, but the collapse of the data is not very good. Similar results have been obtained in the two-dimensional RFM. The postpeak damage profiles display exponential tails; however, the localization length scales as $\xi \sim L^{0.8}$ [36].

The diffusive and localization behavior of accumulated damage in the pre- and postpeak regimes can also be inferred from an analysis of the widths of the damage cloud in the pre- and postpeak regimes. The width of the damage cloud is defined as $W \equiv [\langle (z_b - \bar{z_b})^2 \rangle]^{1/2}$, where z_b is the z coordinate of a broken bond and the average is taken over different realizations. The measured width of damage cloud at peak load scales as $W \sim L$ (see Fig. 4). This result is consistent with the hypothesis that the damage is uniformly distributed (diffusive) at the peak load and localization occurs in the postpeak regime. The uniform distribution of damage at the peak load results in a scaling of the form $W \simeq L/\sqrt{12} \sim 0.288L$ that is in excellent agreement with the numerical data (see Fig. 4). The width of damage cloud in the postpeak regime scales as $W \sim L^{0.7}$, and this nontrivial scaling exponent indicates that the damage profiles exhibit a localized behavior in the postpeak regime.

Another interesting quantity to study is the scaling of the final crack width. Figure 4 indicates that the final crack width scales as $W \sim L^{0.5}$, which is consistent with the scaling of localization length $\xi \sim L^{0.5}$ used in the data collapse of damage profiles in the postpeak regime. The center of mass shifting of the damage profiles for the purpose of averaging the damage profiles makes this consistency between the final crack width and the localization length ξ of the damage profiles self-evident. In addition, this consistency supports the idea that the postpeak damage profile is predominantly due to the localization produced by the catastrophic failure, which at the same time results in the formation of the final crack. Similar behavior is observed in two-dimensional RFM; namely, the width of the damage cloud in the prepeak regime is consistent with the uniform damage profile, and that the scaling of final crack width ($\sim L^{0.81}$, see Fig. 11 of Ref. [36]) is consistent with the scaling of localization length $\xi \sim L^{0.8}$ (see Fig. 9 of Ref. [36]) of the postpeak damage profiles. Interestingly, the same consistency in scaling between the final crack width and the localization length of the postpeak damage profiles is observed in the random spring models as well. The final crack width scales as $W \sim L^{0.64}$ (see Ref. [38]), and the localization length ξ of the postpeak damage profiles scales as $\xi \sim L^{0.65}$ (see Fig. 6 of Ref. [37]).

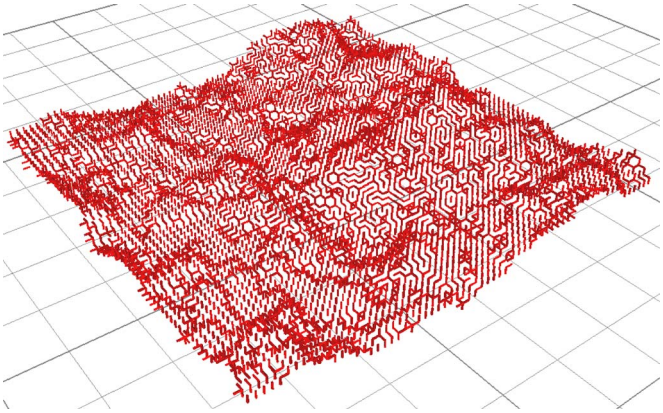

FIG. 5. (Color online) Crack surface in a typical cubic lattice system of size $L=64$.

IV. CRACK SURFACE ROUGHNESS

Once the complete fracture of the lattice system has occurred, we identify the final crack by removing the dangling ends and overhangs as shown in Fig. 5. The crack surface is represented by a single valued height function $z(x,y)$ in the $x-y$ reference plane, where $x \in [0,L]$ and $y \in [0,L]$. Several methods have been devised to characterize the roughness of an interface and their reliability has been tested against synthetic data [39]. If the interface is self-affine, all the methods should yield the same result in the limit of large samples. For instance, consider the local crack width of a crack line $z(x,y=c)$. The local width using the variable bandwidth method is computed as $w(\ell) \equiv \langle \Sigma_x [z_x - (1/\ell)\Sigma_X z_X]^2 \rangle^{1/2}$, where the sums are restricted to windows of length ℓ along the x direction and the average $\langle \cdots \rangle$ is taken over all possible origins of the windows along the profile, and over different realizations. The self-affine scaling properties of crack surfaces results in a scaling law of form $w(\ell) \sim \ell^{\zeta}$ for $\ell \ll L$ that saturates to a value $W = w(L) \sim L^{\zeta}$ corresponding to the global width. A more precise value of the exponents is obtained from the power spectrum, which is expected to

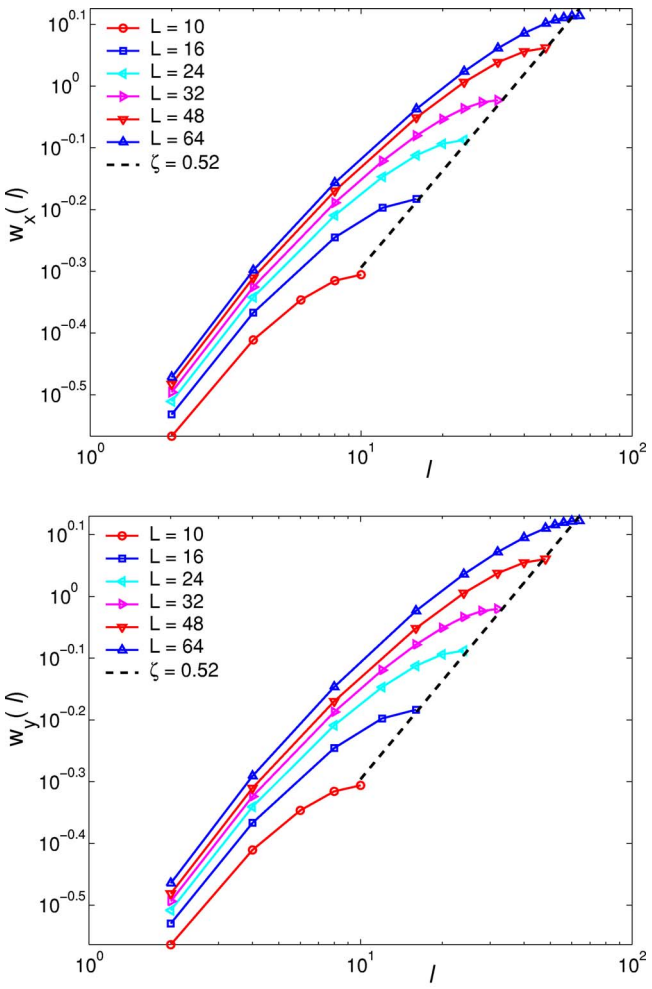

FIG. 6. (Color online) The local width $w(l)$ of the crack in the x and y directions for different lattice sizes in log-log scale. The crack width scaling in x and y directions is identical. The global width yields a scaling exponent $\zeta=0.52$.

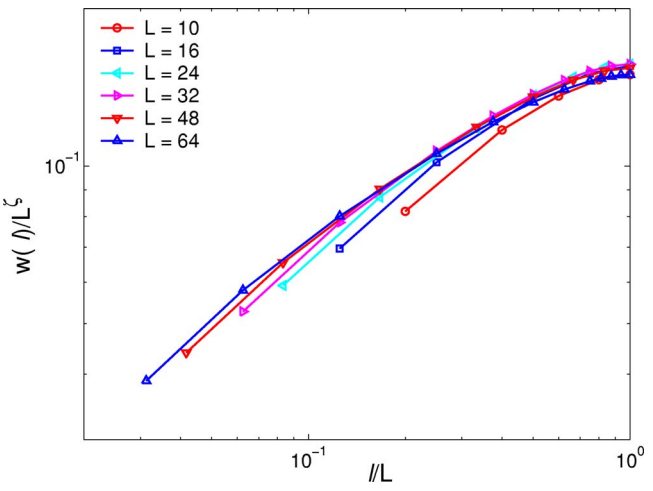

FIG. 7. (Color online) The collapse of the local crack widths in the x direction with $\zeta=0.52$. The collapse of the data, however, is not very good. The scenario for the collapse of local crack widths in y direction is similar.

yield more precise estimates [39]. The power spectrum or the structure factor is computed as $S(k)\equiv\langle\hat{z}_k\hat{z}_{-k}\rangle/L$, where $\hat{z}_k\equiv\Sigma_x z_x \exp(2\pi ixk/L)$, and decays as $S(k)\sim k^{-(2\zeta+1)}$.

We estimate the crack surface roughness in the x and y directions by considering number of slices along each direction. For instance, the crack roughness in the x direction is computed by considering the roughness of $L+1$ number of slices, each with $z(x,y=c)$, where c is a constant that takes on values $c=1,2,\ldots,L+1$. Once the crack line roughness of each of these $L+1$ lines with $z(x,y=c)$ is computed, the crack surface roughness in the x direction is estimated as the average roughness of these $L+1$ crack lines, which is then averaged over different realizations. Similarly, the crack surface roughness in the y direction is computed as the average roughness of the $L+1$ crack lines $z(x=c,y)$, where c is a constant that takes on values $c=1,2,\ldots,L+1$ for each of the $L+1$ slices, respectively.

Figure 6 presents the scaling of local crack width in the x and y directions for different lattice system sizes. The results presented in Figs. 6(a) and 6(b) indicate that the crack width scaling in the x and y directions is identical. A reference line, obtained by fitting the scaling of the global width with L, indicates a roughness exponent $\zeta=0.52$. We have obtained the same scaling exponents in both x and y directions. It should be noted that the exponent $\zeta=0.52$ differs slightly from the global crack width exponent of $\zeta=0.5$ presented in Fig. 4. The reason for this discrepancy is that the crack width exponent in Fig. 4 is calculated as $W=\langle\Sigma(z-\bar{z})^2\rangle^{1/2}$ for the entire crack surface $z(x,y)$, whereas the global width exponent in Fig. 6 is averaged over $L+1$ crack lines of $z(x,y=c)$ with $c=1,2,\ldots,L+1$. It should also be noted that the exponent $\zeta=0.52$ differs considerably from the exponent $\zeta=0.62\pm0.05$ proposed in [27,34,35] and that of $\zeta=0.41\pm0.02$ proposed in [29]. However, the difference may be due to the fewer number of statistical samples considered in these earlier studies.

A direct fit of the local width based on Figs. 6(a) and 6(b) would not be reliable due to the very small scaling regime. Thus, in Fig. 7 we present the collapse of the local crack width data using the scaling form $w(\ell)\sim\ell^{\zeta}f(\ell/L)$ and the result is not very good.

In two-dimensional RFM, our data with improved statistics and large system sizes [22] indicated that the crack roughness scaling is anomalous [9]. In previous measurements on two-dimensional RFM, anomalous scaling could not be detected since the data was available only for smaller system sizes. Anomalous scaling has been observed not only in various growth models [9] but also in fracture surfaces in granite [10] and wood samples [11]. Anomalous scaling implies that the exponent describing the system size dependence of the surface *differs* from the local exponent measured for a fixed system size L. In particular, the local width scales as $w(\ell)\sim\ell^{\zeta_{loc}}L^{\zeta-\zeta_{loc}}$, so that the global roughness W scales as L^{ζ} with $\zeta>\zeta_{loc}$. Consequently, the power spectrum scales as $S(k)\sim k^{-(2\zeta_{loc}+1)}L^{2(\zeta-\zeta_{loc})}$. The upward shift of the $w(\ell)$ presented in Figs. 6(a) and 6(b) for different system sizes is a fingerprint of anomalous scaling, since such a shift indicates that $w(\ell)$ grows with L. This is a key feature of anomalous scaling that can be spotted by just looking at the

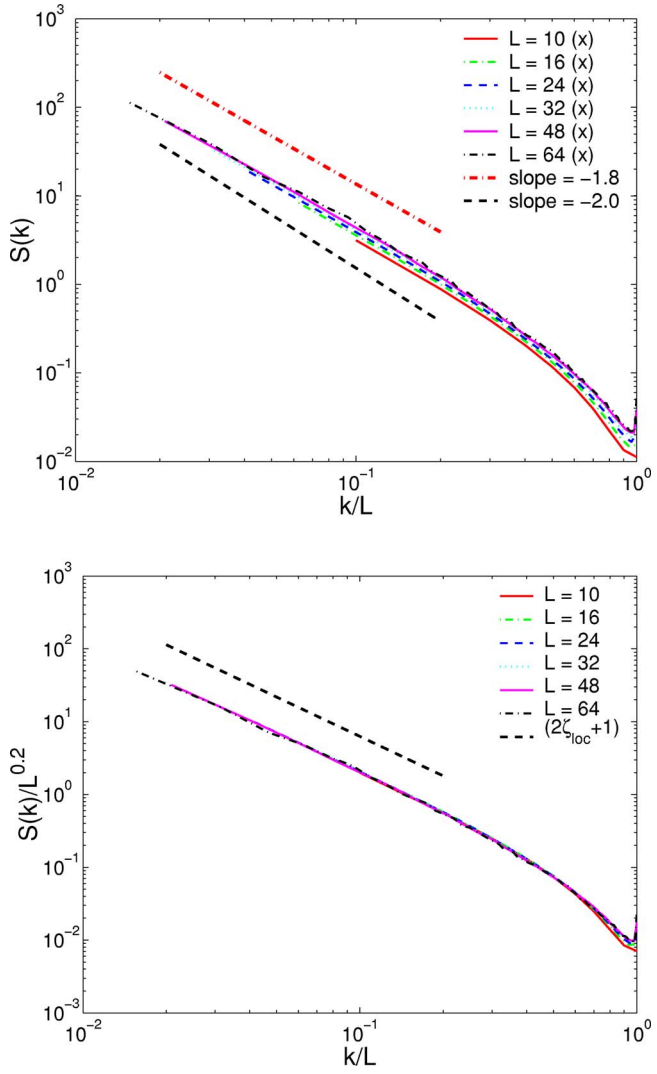

FIG. 8. (Color online) The power spectrum of the crack $S(k,L)$ in x direction for different lattice sizes in log-log scale. (a) Uncollapsed power spectrum data. The collapse of the data is not perfect, and the slope of the spectra is equal to −1.80. A line with a slope of $-(2\zeta+1)=-2.0$ is provided for reference. (b) The spectra for all of the different lattice sizes can be collapsed by normalizing $S(k,L)$ with $L^{2(\zeta-\zeta_{loc})}$, where $(\zeta-\zeta_{loc})=0.1$. The slope defines the local exponent as $-(2\zeta_{loc}+1)$ and is equal to −1.80, implying that $\zeta_{loc}=0.4$ and $\zeta=0.5$. Identical exponents are obtained using the power spectrum data in y direction.

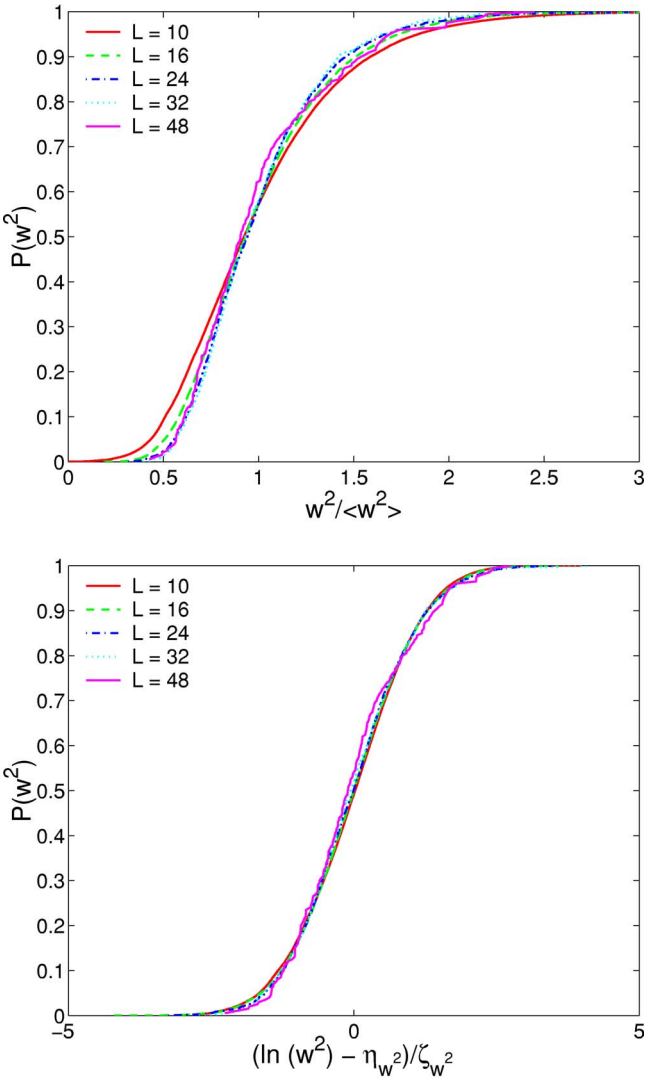

FIG. 9. (Color online) Crack width distributions for different lattice sizes. (a) Deviations are observed from the scaling form $P(W^2)=P(W^2/\langle W^2\rangle)$. (b) The collapsed distribution of crack widths obtained using the reduced variable $\bar{\xi}_{W^2}=\frac{\ln(W^2)-\eta_{W^2}}{\zeta_{W^2}}$.

local roughness amplitudes. In order to further check the presence of anomalous scaling in three dimensions, we report in Figs. 8(a) and 8(b) the x-direction data collapse of the power spectra for different system sizes. Identical results are obtained using the power-spectrum data in the y direction. Figure 8(a) presents the uncollapsed power spectrum data and two reference lines with slopes of $-(2\zeta_{loc}+1)=-1.8$ and $-(2\zeta+1)=-2.0$. Clearly, the collapse of the data in Fig. 8(a) is not perfect; there appear to be small but systematic shifts in the data with system sizes. Also, the reference line with a slope of $-(2\zeta+1)=-2.0$ (corresponding to a global roughness exponent of $\zeta=0.5$) is not a good fit, which suggests the presence of anomalous scaling. On the other hand, a perfect data collapse is obtained in Fig. 8(b) using the anomalous scaling form $S(k)\sim k^{-(2\zeta_{loc}+1)}L^{2(\zeta-\zeta_{loc})}$, with $\zeta-\zeta_{loc}=0.1$. A straight line fit of the power law decay of the spectrum yields an estimate for the local roughness exponent equal to $\zeta_{loc}=0.4$, which implies a global roughness exponent of $\zeta=0.5$, since $\zeta-\zeta_{loc}=0.1$. Clearly, the global roughness exponents obtained using the variable bandwidth method (0.52) and the power spectrum method (0.5) are in excellent agreement, and the small difference can be attributed to the bias associated to the methods employed [39]. Although the value of $\zeta-\zeta_{loc}$ as estimated using the power spectrum method is small, it is significantly larger than zero and it may even correspond to a logarithmic growth. However, based on our numerical results, which included lattice system sizes up to $L=64$ with extensive statistical sampling, it is not possible to conclude with certainty whether anomalous scaling of crack surface roughness is present in three-dimensional RFM or not. Simulations on much larger lattice systems are anticipated to clarify this.

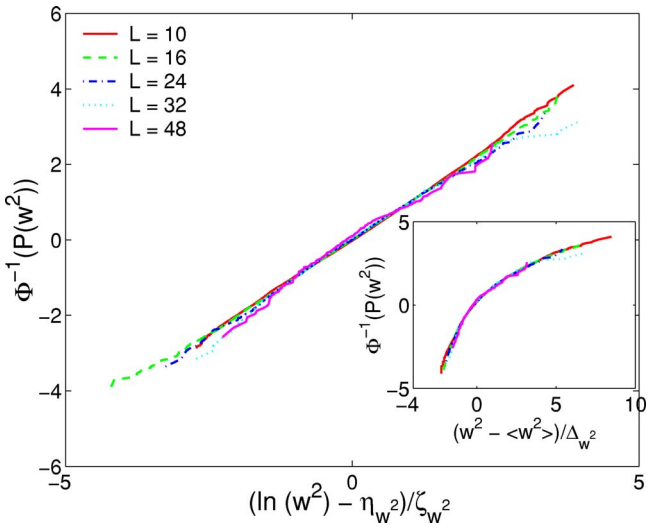

FIG. 10. (Color online) The collapse of the crack width distribution data onto a straight line suggests that it follows a lognormal distribution. The inset shows that a Gaussian distribution is not an adequate fit for the crack width distribution.

V. CRACK WIDTH DISTRIBUTION

We have analyzed the probability density distribution $p(W^2)$ of the global crack width. This distribution has been measured for various interfaces in models and experiments and typically rescales as [40]

$$p(W^2) = p(W^2/\langle W^2\rangle)/\langle W^2\rangle, \tag{2}$$

where $\langle W^2\rangle \sim L^{2\zeta}$ is the average global width. Equation (2) implies that the corresponding cumulative distribution $P(W^2)$ of crack global width scales as $P(W^2)=P(W^2/\langle W^2\rangle)$. Figure 9(a) shows that a reasonable collapse of the crack global width distributions for different lattice system sizes may be achieved using Eq. (2). However, the data collapse is not perfect, and deviations from the scaling $P(W^2)=P(W^2/\langle W^2\rangle)$ are evident. Alternatively, an excellent collapse of the data is obtained in Fig. 9(b) using the reduced log-normal coordinate $\bar{\xi}_{W^2}=\frac{\ln(W^2)-\eta_{W^2}}{\zeta_{W^2}}$, where η_{W^2} and ζ_{W^2} denote the mean and standard deviation of logarithm of W^2. In Fig. 10, a reparametrized form of the log-normal distribution is presented. The collapse of the data onto a straight line indicates that the log-normal distribution represents an excellent fit to the distribution of crack global widths. We have also tried a Gaussian fit for the distribution of crack global widths. The inset of Fig. 10 presents a Gaussian fit for the crack global widths distribution wherein significant curvature in the collapsed plots can be observed. This suggests that the normal distribution is not as good a fit as the log-normal distribution for the crack global width distribution. Finally, in Ref. [22], it is shown that the crack width distributions in the two-dimensional RFM are also well fit by a log-normal distribution for both diamond and triangular lattices of different system sizes. The data collapse and log-normality of crack width distributions in three-dimensional RFM as well as in two-dimensional RFM for different lattice topologies suggests universality of crack width distributions.

VI. CONCLUSIONS

In this paper we have analyzed the localization properties of fracture in the three-dimensional random fuse model using an improved statistical sampling and larger lattices than what was previously done in the past. We have analyzed the roughness of the final crack and found a local exponent $\zeta_{loc}=0.4$, which is slightly different from the global roughness exponent $\zeta=0.52$. A similar difference between local and global exponents was also found in two-dimensional simulations for both triangular and diamond lattices [22], suggesting that anomalous scaling is a generic feature of the fracture of disordered media, as already found in fracture experiments [10]. The numerical value of the exponents is, however, quite far from the three-dimensional experimental results, indicating that additional physical mechanisms should probably be taken into account. We have also evaluated the width distribution [40] that can be collapsed into a single curve for different lattice sizes and it appears to be well fit by a lognormal distribution. Finally, the analysis of damage profiles indicates that the localization process occurs abruptly after peak load.

In summary, the present results seem to indicate that the RFM provides only a qualitative description of the fracture surface morphology found in experiments. The quantitative differences may be attributed to the strong simplifications present in the model such as its scalar nature, the quasistatic dynamics, and the absence of a pre-existing notch; although a roughness exponent of $\zeta=0.5$ [30] is obtained using three-dimensional Born model as well. On the other hand, the initial phase of damage accumulation leading to localization and failure in a strongly disordered sample are well captured by the RFM model, but further work is needed to clarify these issues.

ACKNOWLEDGMENTS

This research is sponsored by the Mathematical, Information and Computational Sciences Division, Office of Advanced Scientific Computing Research, U.S. Department of Energy, under contract number DE-AC05-00OR22725 with UT-Battelle, LLC. S.Z. is thankful for hospitality provided by the Kavli Institute for Theoretical Physics where this work was completed and also acknowledges partial financial support through NSF Grant No. PHY99-07949.

[1] *Statistical Models for the Fracture of Disordered Media*, edited by H. J. Herrmann and S. Roux (North-Holland, Amsterdam, 1990); *Non-Linearity and Breakdown in Soft Condensed Matter*, edited by K. K. Bardhan, B. K. Chakrabarti, and A. Hansen (Springer Verlag, Berlin, 1994); B. K. Chakrabarti and L. G. Benguigui, *Statistical Physics of Fracture and Breakdown in Disordered Systems* (Oxford University Press, Oxford, 1997). D.Krajcinovic and van Mier, *Damage and Fracture of Disordered Materials* (Springer Verlag, New York, 2000).

[2] B. B. Mandelbrot, D. E. Passoja, and A. J. Paullay, Nature (London) **308**, 721 (1984).

[3] B. B. Mandelbrot, Phys. Scr. **32**, 257 (1985).

[4] For a review, see E. Bouchaud, J. Phys.: Condens. Matter **9**, 4319 (1997); E. Bouchaud, Surf. Rev. Lett. **10**, 73 (2003).

[5] K. J. Maloy, A. Hansen, E. L. Hinrichsen, and S. Roux, Phys. Rev. Lett. **68**, 213 (1992); E. Bouchaud, G. Lapasset, J. Planés, and S. Navéos, Phys. Rev. B **48**, 2917 (1993).

[6] P. Daguier, B. Nghiem, E. Bouchaud, and F. Creuzet, Phys. Rev. Lett. **78**, 1062 (1997).

[7] J. Schmittbuhl, S. Roux, and Y. Berthaud, Europhys. Lett. **28**, 585 (1994); J. Schmittbuhl, F. Schmitt, and C. Scholz, J. Geophys. Res. **100**, 5953 (1995).

[8] J. J. Mecholsky, D. E. Passoja, and K. S. Feinberg-Ringel, J. Am. Ceram. Soc. **72**, 60 (1989).

[9] J. M. López, M. A. Rodríguez, and R. Cuerno, Phys. Rev. E **56**, 3993 (1997).

[10] J. M. López and J. Schmittbuhl, Phys. Rev. E **57**, 6405 (1998).

[11] S. Morel, J. Schmittbuhl, J. M. López, and G. Valentin, Phys. Rev. E **58**, 6999 (1998).

[12] L. de Arcangelis, S. Redner, and H. J. Herrmann, J. Phys. (Paris), Lett. **46**, 585 (1985).

[13] M. Sahimi and J. D. Goddard, Phys. Rev. B **33**, 7848 (1986).

[14] B. Kahng, G. G. Batrouni, S. Redner, L. de Arcangelis, and H. J. Herrmann, Phys. Rev. B **37**, 7625 (1988).

[15] L. de Arcangelis, A. Hansen, H. J. Herrmann, and S. Roux, Phys. Rev. B **40**, 877 (1989).

[16] A. Delaplace, G. Pijaudier-Cabot, and S. Roux, J. Mech. Phys. Solids **44**, 99 (1996).

[17] S. Zapperi, P. Ray, H. E. Stanley, and A. Vespignani, Phys. Rev. Lett. **78**, 1408 (1997); Phys. Rev. E **59**, 5049 (1999).

[18] A. Hansen and S. Roux, in *Damage and Fracture of Disordered Materials*, edited by D. Krajcinovic and van Mier (Springer Verlag, New York, 2000) pp. 17–101.

[19] A. Hansen, E. L. Hinrichsen, and S. Roux, Phys. Rev. Lett. **66**, 2476 (1991).

[20] E. T. Seppälä, V. I. Räisänen, and M. J. Alava, Phys. Rev. E **61**, 6312 (2000).

[21] J. O. H. Bakke, J. Bjelland, T. Ramstad, T. Stranden, A. Hansen, and J. Schmittbuhl, Phys. Scr. **T106**, 65 (2003).

[22] S. Zapperi, P. K. V. V. Nukala, and S. Simunovic, Phys. Rev. E **71**, 026106 (2005).

[23] G. Mourot, S. Morel, E. Bouchaud, and G. Valentin, Phys. Rev. E **71**, 016136 (2005).

[24] C. Poirier, M. Ammi, D. Bideau, and J. P. Troadec, Phys. Rev. Lett. **68**, 216 (1992).

[25] T. Engoy, K. J. Maloy, A. Hansen, and S. Roux, Phys. Rev. Lett. **73**, 834 (1994).

[26] J. Kertész, V. K. Horváth, and F. Weber, Fractals **1**, 67 (1993); J. Rosti, L. I. Salminen, E. T. Seppälä, M. J. Alava, and K. J. Niskanen, Eur. Phys. J. B **19**, 259 (2001); L. I. Salminen, M. J. Alava, and K. J. Niskanen, Eur. Phys. J. B **32**, 369 (2003).

[27] G. G. Batrouni and A. Hansen, Phys. Rev. Lett. **80**, 325 (1998).

[28] V. I. Räisänen, M. J. Alava, and R. M. Nieminen, Phys. Rev. B **58**, 14288 (1998).

[29] V. I. Räisänen, E. T. Seppälä, M. J. Alava, and P. M. Duxbury, Phys. Rev. Lett. **80**, 329 (1998).

[30] A. Parisi, G. Caldarelli, and L. Pietronero, Europhys. Lett. **52**, 304 (2000).

[31] A. Hansen, E. L. Hinrichsen, and S. Roux, Phys. Rev. B **43**, 665 (1991).

[32] P. K. V. V. Nukala and S. Simunovic, J. Phys. A **36**, 11403 (2003).

[33] P. K. V. V. Nukala and S. Simunovic, J. Phys. A **37**, 2093 (2003).

[34] A. Hansen and J. Schmittbuhl, Phys. Rev. Lett. **90**, 045504 (2003).

[35] T. Ramstad, J. O. H. Bakke, J. Bjelland, T. Stranden, and A. Hansen, Phys. Rev. E **70**, 036123 (2004).

[36] P. K. V. V. Nukala, S. Simunovic, and S. Zapperi, J. Stat. Mech.: Theory Exp. 2004, P08001.

[37] P. K. V. V. Nukala, S. Zapperi, and S. Simunovic, Phys. Rev. E **71**, 066106 (2005).

[38] G. Caldarelli, R. Cafiero, and A. Gabrielli, Phys. Rev. E **57**, 3878 (1998).

[39] J. Schmittbuhl, J. P. Vilotte, and S. Roux, Phys. Rev. E **51**, 131 (1995).

[40] G. Foltin, K. Oerding, Z. Rácz, R. L. Workman, and R. K. P. Zia, Phys. Rev. E **50**, R639 (1994); M. Plischke, Z. Rácz, and R. K. P. Zia, Phys. Rev. E **50**, 3589 (1994); Z. Rácz and M. Plischke, Phys. Rev. E **50**, 3530 (1994); T. Antal, M. Droz, G. Györgyi, and Z. Rácz, Phys. Rev. Lett. **87**, 240601 (2001); T. Antal, M. Droz, G. Györgyi, and Z. Rácz, Phys. Rev. E **65**, 046140 (2002); A. Rosso, W. Krauth, P. Le Doussal, J. Vannimenus, and K. J. Wiese, Phys. Rev. E **68**, 036128 (2003).